Research Square

Preprints are preliminary reports that have not undergone peer review.
They should not be considered conclusive, used to inform clinical practice,
or referenced by the media as validated information.

# Device Optimization of Non-Ideal Ion-Sensitive Back Barrier β-(AlGa)2O3/Ga2O3 HEMT for pH Sensor application

**Ravi Ranjan**
Dr. B. R. Ambedkar National Institute of Technology Jalandhar
**Dr. Nitesh Kashyap**
Dr. B. R. Ambedkar National Institute of Technology Jalandhar
**Dr. Ashish Raman**
Dr. B. R. Ambedkar National Institute of Technology Jalandhar
**Dr. Naveen Kumar**
University of Glasgow
**Dr. Prateek Kumar**
Dr. B. R. Ambedkar National Institute of Technology Jalandhar
**Dr. Sarabdeep Singh**
sarabdeep1611@gmail.com

Model Institute of Engineering and Technology Jammu

**Research Article**

**Keywords:** pH sensor, Analytical Model, ISFET, HEMT. 2DEG, Electrolyte

**Posted Date:** April 28th, 2026

**DOI:** https://doi.org/10.21203/rs.3.rs-9396349/v1

**License:** This work is licensed under a Creative Commons Attribution 4.0 International License.
Read Full License

**Additional Declarations:** No competing interests reported.

**Version of Record:** A version of this preprint was published at Applied Physics A on September 3rd, 2026. See the published version at https://doi.org/10.1007/s00339-026-10158-4.

# Device Optimization of Non-Ideal Ion-Sensitive Back Barrier β-$(AlGa)_2O_3/Ga_2O_3$ HEMT for pH Sensor application

Ravi Ranjan, Nitesh Kashyap, Ashish Raman, Naveen Kumar, Prateek Kumar and Sarabdeep Singh

***Abstract*— We analyzed a mathematical model using commercial Silvaco and MATLAB tools to study the non-ideal behavior of a back barrier β-$(AlGa)_2O_3/Ga_2O_3$ ion-sensitive HEMT based pH sensor around its isoelectric point. In this model, $Al_2O_3$ serves as the dielectric between the $(AlGa)_2O_3$ layer of HEMT and the electrolyte, functioning as the sensing membrane. An electrolyte concentration of 1 mM was used for the mathematical modeling and simulation, as lower concentrations enhance sensor sensitivity. To better understand the behavior of the electrical double layer in interaction with the electrolyte, we employed the Gouy-Chapman-Stern and site-binding theories. In a strongly acidic medium, the pH sensor exhibits non-linear behavior. This paper presents an analysis of the analog and linearity performance of the pH sensor, focusing on design parameters such as gate length and gate work function. For improved performance, a larger threshold voltage is necessary for β-$(AlGa)_2O_3/Ga_2O_3$ HEMT for high-power devices, while a high $I_{ON}/I_{OFF}$ ratio is essential for better sensor performance. All simulated results (analog and linearity) were analyzed for a pH range of 0 to 14. The pH value was found to depend on the device parameters. We investigated the effects of pH variation on transfer characteristics, $I_{ON}/I_{OFF}$ ratio, $I_{OFF}$, and threshold voltage, with respect to gate length and gate work function. The sensor performed optimally at a gate length of 1.2 μm and a work function of 6 eV, achieving an $I_{ON}/I_{OFF}$ ratio of $10^7$ and a threshold voltage of 1.6 V.***

***Index Terms*— pH sensor, Analytical Model, ISFET, HEMT. 2DEG, Electrolyte**

## I. INTRODUCTION

In the last few decades, Due to fast response time and easy on-chip integration of FET-based sensors, their demands are continuously enhancing biomolecule detection. One of the diagnostic biomarkers in the human body is the pH value, which determines several biomolecule diseases. Therefore, there is a lot of interest in the scientific community for biosensors for pH detection. In the health care and life sciences, biosensors use in many places, such as blood monitoring, glucose monitoring and pathogens detection [1-2].

P. Bergveld has described the first FET-based pH sensor based on an ion-sensitive FET (ISFET). This work was described in 1972 [3]. ISFETs, which have the highest precision and degree of miniaturization, are used to monitor acidity. ISFETs use a capacitance effect to transduce the ion activity in the solvent and measure the associated charge.

Depending on the bulk concentration and the affinities of the capacitance, which contributes to the formation of the final signal [4-6]. ISFETs have many uses, including monitoring the enzymatic activity of polymerase to help with DNA sequencing, sweat biomarker sensors, physiological measures, and more [7-10]. Many FET-based biosensors [11-12] are developed for the detection of glucose [13], Uric acid [1,14], protein and lactic acid [15-16], which are being used for monitoring environment management, food quality and biomedical applications [17]. Sensors related to FET devices have also been used for the detection of various other biomolecule species, such as anthrax [18], glucose [19] and c-reactive protein [11]. Modulation doped β-$(AlGa)_2O_3/Ga_2O_3$ (β -AGO/GO) are mostly used in high-power RF applications, but because of their excellent stability and ability to quickly bond with polar liquids, they also produce high-quality sensors in the industrial and medical fields [20–21]. The β -AGO/GO High electron mobility transistor (HEMT) has outstanding performance as a sensor at high temperatures, severe environments, and alkali or acidic solution conditions, and it is mainly used in different sensors such as pH Sensors, gas sensors, biosensors, and pressure sensors [22–24]. In the HEMT, a channel (2DEG) is formed, which is highly sensitive depending on the surface charges. As a result, an ISFET model-based biosensor is developed employing a HEMT device [24]. A layer of oxide in the ISFET model absorbs hydrogen and hydroxyl ions from the electrolyte, producing atmospheric oxides in the solution. Carriers of 2DEG are affected by the change in pH of electrolyte because of change in surface charges takes place [24].

Sentaurus and Silvaco, two commercial TCAD software, have been used to specify the parameters of the electrolyte/oxide and create a physical model for the pH sensor [25, 26]. The TCAD commercial product uses linear models and therefore is only valid under ideal circumstances with a sensitivity factor of 1.

In this paper, the β-AGO/GO-based back barrier layer based pH sensor is simulated by using ISFET based model with an electrolyte placed between the gate metal and oxide, it transduces the information carrying from H+ conc. of an electrolyte solution (pH) into an electrical signal. Here, $Al_2O_3$

is used as an insulator in β-AGO/GO HEMT [24], placed below the electrolyte solution, and used as a sensing membrane. Since HEMT is a high power and voltage device, so it operates upto high potential and only $Al_2O_3$ shows large surface potential range (-0.3 to 0.4 V). So, $Al_2O_3$ is better choice for pH sensor application for HEMT. Also, using MATLAB, we created an analytical model for nonlinear or nonideal pH sensors that provides more accurate measurement results and is experimentally proven. The analytical model has examined the surface potential at various pH ranges between 0 and 14. (Acidic to basic). The simulated result of β-AGO/GO HEMT has been analysed on Silvaco Atlas, and obtained results are analyzed mathematically using MATLAB. Analog (Drain current, $I_{ON}/I_{OFF}$, threshold voltage, transconductance) and linearity parameters are investigated for various pH values (from 0 to 14). The device processes parameters such as gate work function (ϕm) and gate length (LG) are discussed in this manuscript for acidic to basic medium (for pH value 0 to 14).

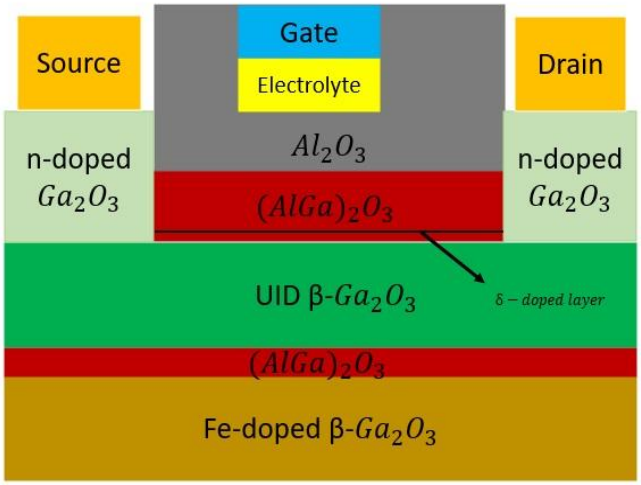



Fig. 1 Schematic of β-(AlGa)2O3/Ga2O3 HEMT with $Al_2O_33$ is used as dielectric.

## II. DEVICE STRUCTURE AND TCAD ANALYTICAL MODEL

β-AGO/GO HEMT is designed using the AGO layer as a barrier layer, which deposits on the GO channel region. The energy bands of both layers are different, and AGO shows a larger energy band than GO. Due to energy band difference, a potential well is created near the interface of two layers, and it is responsible for forming a channel in the form of 2DEG. Below the channel layer, another barrier layer deposites to enhance the performance of 2DEG. 2DEG is highly sensitive to surface potential variation. In the case of the pH sensor, the surface potential varies with a change in the pH value of the electrolyte due to a change in the surface potential of the carrier conc. varies in 2DEG. This type of device is used for the practical application of biosensors.

The length and width of the presented β-AGO/GO HEMT are 6 µm and 2 µm respectively. The substrate of the given device is Fe-doped GO, and the channel region is formed by unintentionally doped (UID) β-GO, as shown in Fig. 1.

Heavily n-doped GO up to the AGO and GO interface forms the source and drain area. When silicon is doped with a (donor concentration ~5×1012 cm-2), 2DEG is created and deposited 4 nm above the interface of β-GO.

Source and drain regions are formed by heavily n-doped GO up to the interface of AGO and GO. 2DEG is formed by delta doping of silicon, with is deposited 4nm above the interface of β-GO. This layer is used as a spacer layer to enhance the channel mobility of the device. The physical parameters of the device have given in table I.

$Al_2O_3$ is used as a dielectric above the barrier layer and as a sensing membrane for the pH sensor. An electrolyte is placed between the dielectric and gate metal to check the pH sensitivity. The surface charges at the oxide and electrolyte interface varies with the electrolyte's pH value changes. Simulation of the device is done on a gate length of 900 nm, a gate work function of 5.93eV, and a source/drain work function of 3.9eV. All the simulation are carried out at gate Voltage (VGS)=5V and Drain Voltage (VDS)=5V.

Table I. Parameter used for device simulations.

| Parameters | AGO/GO HEMT |
|---|---|
| Gate Length, LG (nm) | 900 |
| Gate oxide thickness, tox (nm) | 5 |
| Device length (nm) | 6000 |
| ϕG (eV) | 5.93 |
| ϕS,D (eV) | 3.9 |
| Delta Doping (cm-3) | $5*10^{12}$ |
| (AlGa)2O3 thickness (nm) | 27 |
| Electrolyte thickness (nm) | 10 |
| Back Barrier layer (nm) | 12 |

ISFET-based TCAD model has been developed for pH sensors at the interface of electrolyte and gate oxide ($Al_2O_3$), and it gives the relation between the variation of the behaviour of oxide with pH of the electrolyte. A sensing membrane (oxide) that recognizes biological events and a transducer that converts the signal from the detected biological event into an electrical signal are components of an ISFET-based structure [3, 27]. ISFET measures the capacitive effects of the associate charges present in the solvent (electrolyte). The efficiency of the interaction of ions of the electrolyte with oxide depends upon the bulk concentration and the material interface's affinity [28-30]. Electrical signal flows from the double-layer capacitance are responsible for the formation of charged particles.

The first developed model of ISFET given by Bergveld [3], has generated the relation between drain current and electrostatic potential, $\Psi 0$. $\Psi 0$ related to the pH value of the electrolyte. At the interface of the oxide and electrolyte solution, a surface reaction occurs, which changes the behaviour of the oxide. Due to the reaction at the interface, charges are generated at the oxide, and it develops electrostatic potential $\Psi 0$ near the oxide surface [24]. According to the mathematical Eq. (1), a difference in H+ concentration between the electrolyte's bulk and surface is caused by the potential difference between an oxide (in this case, $Al_2O_3$) and an electrolyte solution [29].

$$pHS = pHB + \frac{q\Psi_0}{2.3KT} \quad (1)$$

pHS and pHB represent the pH value at the surface and bulk, respectively. q, T, K are the elementary charge, temperature, and Boltzmann constant, respectively. With the help of Eq.1, we can analyze that there is a different value of H+ conc. at the surface and bulk of the electrolyte.

Diffusion capacitance [24], Cdif is determined by Eq (2) and is defined as the ability of the solution to vary the number of reverse charges in response to a slight change in $\Psi_0$. Its value is zero at the pH of the point-of-zero-charge (pHpzc), as a result of the adsorption of H+ ions in the oxide surface. At the point-of-zero-charge, adsorption and desorption processes are in equilibrium and they can be analysed from their respective affinities pKa and pKb that is ($pHpzc = \frac{pK_a + pK_b}{2}$). Potential with respect to pH is described by Eq. (3) [24].

When the dielectric layer comes into contact with the electrolyte, the buffering capacity of a chemical determines the sensitivity parameter (α), which determines how the ions in solution react and produce the double layer capacitance or CDL. The optimum value is one, and at this value, the surface potential is at its theoretical maximum in relation to pH.

When the sensor exhibits nonideal behaviour, the iterative technique can be used to examine sensitivity (and its value ranges from 0 to 1) with Ψ0 and is determined by the dissociation model and Gour-Chapman-Stern theory [24]. The nonideal behaviour of the sensor has been thoroughly discussed by Eq. (3), and Cdif depends on the properties of the electrolyte such as double layer and stern capacitance [24-25]. When the sensor exhibits non-ideal behaviour, the iterative technique can be used to examine sensitivity (and its value ranges from 0 to 1) with $\Psi_0$ and is determined by the dissociation model and Gour-Chapman-Stern theory [24]. The non-ideal behaviour of the sensor has been thoroughly discussed by Eq. (3) and Cdif depends on the properties of the electrolyte such as double layer and stern capacitance [24-25].

$$\frac{\delta\sigma_0}{\delta\Psi_0} = -C_{dif} \quad (2)$$

$$\frac{\delta\Psi_0}{\delta pHB} = 2.3\frac{KT}{q}\alpha \quad (3)$$

$$\alpha = \frac{1}{\frac{2.3KTC_{dif}}{q^2\beta_{int}}+1} \quad (4)$$

$$\frac{q\Psi_0}{KT} = [2.303(pHpzc - pHB)] - sinh^{-1}\left(\frac{\sigma_{pH}}{2qN_s\sqrt{\frac{K_b}{K_a}}}\right) + \ln\left(1 - \frac{\sigma_{pH}}{qN_s}\right) \quad (5)$$

$$\frac{q\Psi_0}{KT} = [2.303(pHpzc - pHB))] \quad (6)$$

From Eqs. (3), (4) and (5) Cdif, $\beta_{int}$ and α depend upon two factors such as, $\sigma_0$ (surface charge) and potential, $\Psi_0$.

Eq. (6) illustrates the relationship between potential variation and bulk pH (pHB), pHpzc, and Ψ0 under the nonideal case where fluctuates of sensitivity (0 to 1). σ0 is a constant for constant pH. Due to the abrupt change in charge from positive to negative and vice versa at the isoelectric point, Eq. (5) makes

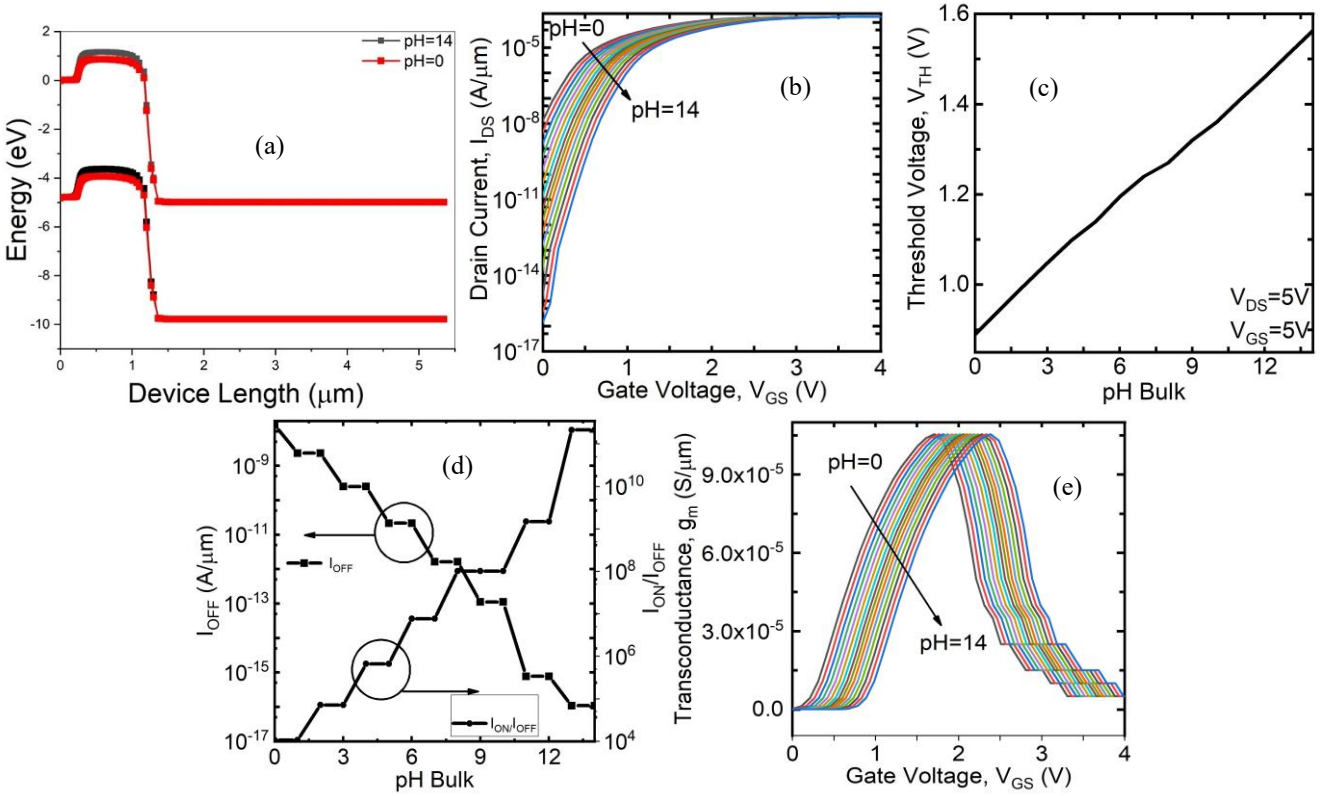



Fig. 2. Analog performance of back barrier β-(AlGa)2O3/Ga2O3 HEMT (a) Transfer characteritics in log scale (a) Transfer characteritics Linear scale (c) Threshold Voltage (d) IOFF and ION/IOFF (d) Transconductance with pH variation from 0 to 14.

it more challenging to determine the precise values of pHB and Ψ0. In order to identify pHB, we employed the extraction procedure. We have altered the potential Ψ0 value in Eq. (5) from -0.3 to 0.4 V for the extraction process (in the case of $Al_2O_3$ dielectric, the value of potential is varied from -0.3 to 0.4 V). $Al_2O_3$ is used as a sensing membrane (dielectric), and its surface density is $8*10^{14}$ (cm-2), permittivity, Ka, Kb, and pHpzc are 9.1, 10, 6 and 8, respectively [24]. We noticed the pH value in the range of 0 to 14 after analyzing in MATLAB for potential Ψ0 with different gate lengths and gate work functions, and the graph is shown in accordance with the analysis. The last two terms of Eq. (5) are ignored in the ideal situation (=1), and the final computation is derived from Eq. (6) [24].

## III. SIMULATION RESULTS AND DISCUSSION

The surface potential of the oxide ($Al_2O_3$) and electrolyte interface varies from -0.3V to 0.4V. $Al_2O_3$ is a better choice as a dielectric in HEMT for pH sensors because of potential variation is larger from negative to positive (-0.3V to 0.4V). Since HEMT is a high-power device, a small surface potential variation does not show better results for different pH. The change in surface potential affects the carrier conc. in the 2DEG and which impacts the performance of the drain current.

When the pH value varies from 0 to 14, than corresponding to that H+ conc. decreases and OH- conc. increases. In an acidic medium or pH value between 0 to 7, the H+ conc. is larger. In this case, the surface potential is positive and therefore needs lower biasing voltage across the gate to reach in saturation condition. At lower pH (0), the H+ conc. is more, and due to this IOFF is lower, and it moves to a large value for pH shifted from acidic to basic medium (0 to 14). Fig. 2. (a) shows the energy band diagram with channel length. Since surface potential of oxide is low at pH = 14 and high at pH=0. Energy band increases with pH and due to this reason low pH (0) sensor will ON in low gate voltage and high gate voltage reuires for pH (14). Transfer characteristics shows in Fig 2 (b) in log scale. In the basic medium, the conc. of H+ is lower and OH- is larger which changes the charge carrier conc. of 2DEG, $I_{OFF}$ current moves from low to high. The ON-State current of the device is 174 mA/mm for all values of pH but the saturation voltage changes for pH to pH. With the increased pH value, transfer characteristics of the presented device are shifted in the right direction. All the simulation works are carried out for drain voltage, $V_{DS}$ = 5V and gate voltage, $V_{GS}$= 4V, after $V_{GS}$ greater than 3.5 V, the ON-State current saturates. ON-state current is almost the same for all pH values because the change in pH does not affect saturation value. Since, In the $I_{DS}$-$V_{GS}$ curve, $I_{DS}$ is shifted in the right direction of the curve, the presented HEMT will change its properties from Normally-ON to Normally-OFF conditions with pH.

The threshold voltage, $V_{TH}$ is the important parameter for all the devices. Power application, there needs a positive $V_{TH}$. $I_{DS}$ shifted from left to right with increasing pH, and so, $V_{TH}$ varies from lower to higher value. The $V_{TH}$ of the device without electrolyte is 1.08 V, but after the addition of electrolyte, the surface potential at the oxide interface varies from -0.21V and 0.48V. So, the resultant $V_{TH}$ of the pH sensor-based device is varied from 0.87 V to 1.56 V for pH (0) and pH (14), respectively, shown in Fig 2 (c). The investigated device gives

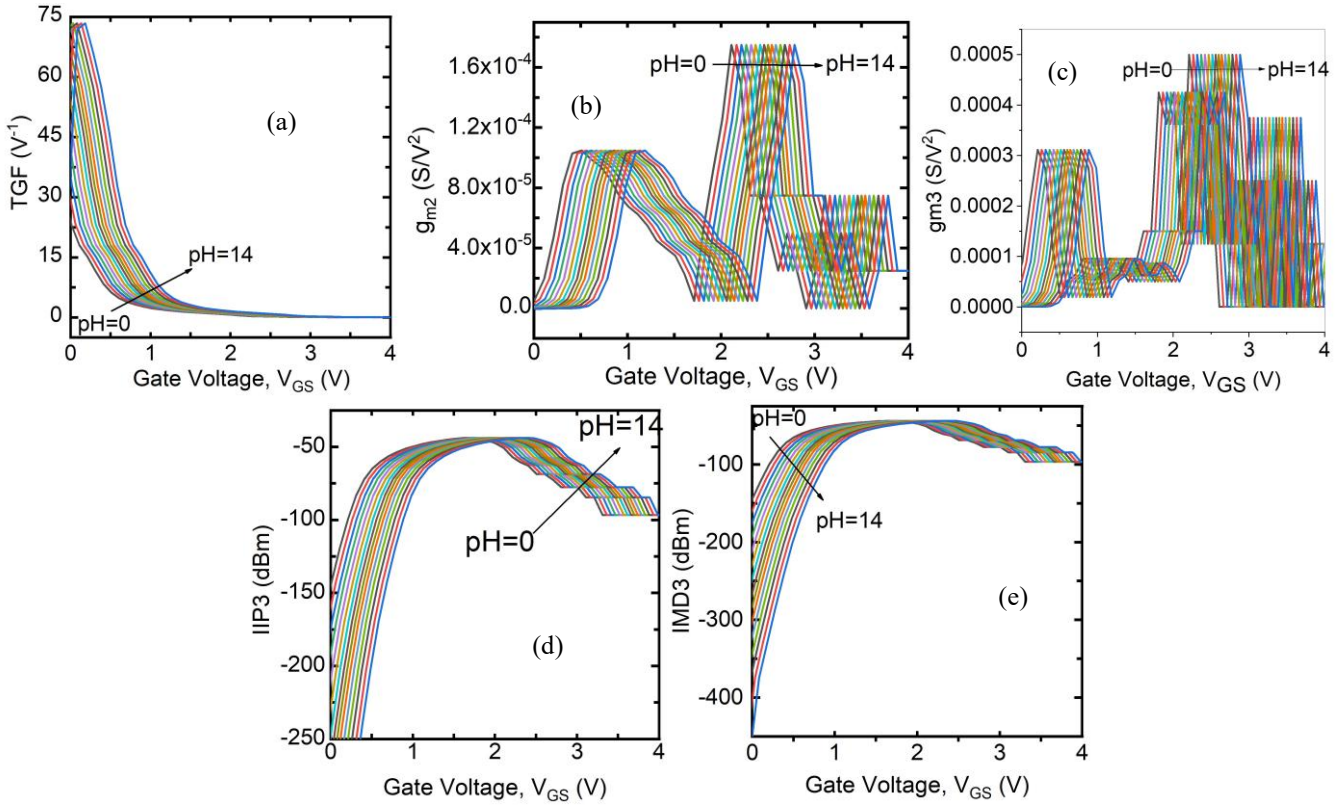



Fig. 3. (a) transconductance generation factor (b) gm2 (c) gm3 (d) IIP3 (e) IMD3 w.r.t gate voltage and variation shows for different value of pH and from 0 to 14.

a threshold voltage sensitivity of 54.3 mV/pH. Fig 2 (d) shows the graph between $I_{ON}/I_{OFF}$ and $I_{OFF}$ with pH value. $I_{ON}/I_{OFF}$ is the main factor of sensor applications. The performance of the Sensor is better if $I_{ON}/I_{OFF}$ is larger. In the presented pH sensor, the $I_{ON}/I_{OFF}$ is increases with variation in pH from lower to higher (0 to 14). Since ON-State current is constant for all pH, but OFF-State current increases with pH. Therefore $I_{ON}/I_{OFF}$ increases with enhancement in pH. $I_{OFF}$ value varies between $10^{-8}$ to $10^{-15}$, and $I_{ON}/I_{OFF}$ switches between 104 to 1011.

Transconductance, gm of the designed pH sensor depends upon the drain current of the device. For lower pH values, current saturates for lower gate bias, and gate bias increases with pH. So, gm reached the maximum value at lower gate bias for lower pH and shifted rightward with increasing pH, as shown in Fig 2 (e). The maximum gm is obtained between 1.5 V and 2.5 V gate bias at pH 0 to 14. gm is an important parameter for linearity analysis. All the parameters of linearity depend on the gm [21].

The transconductance generation factor (TGF), also known as the gm/Ids ratio, determines how effectively the current is used to achieve a specific transconductance value. Higher gm/Ids of the device under study are needed to attain greater analog performance. TGF is inversely related to $I_{DS}$; at lower $V_{GS}$, OFF-state current reduces with increasing pH. TGF reaches its maximum value, and it is equal to 72 V-1 for pH value 14 and is plotted in Fig 3 (a).

The second derivative of the second-order transconductance

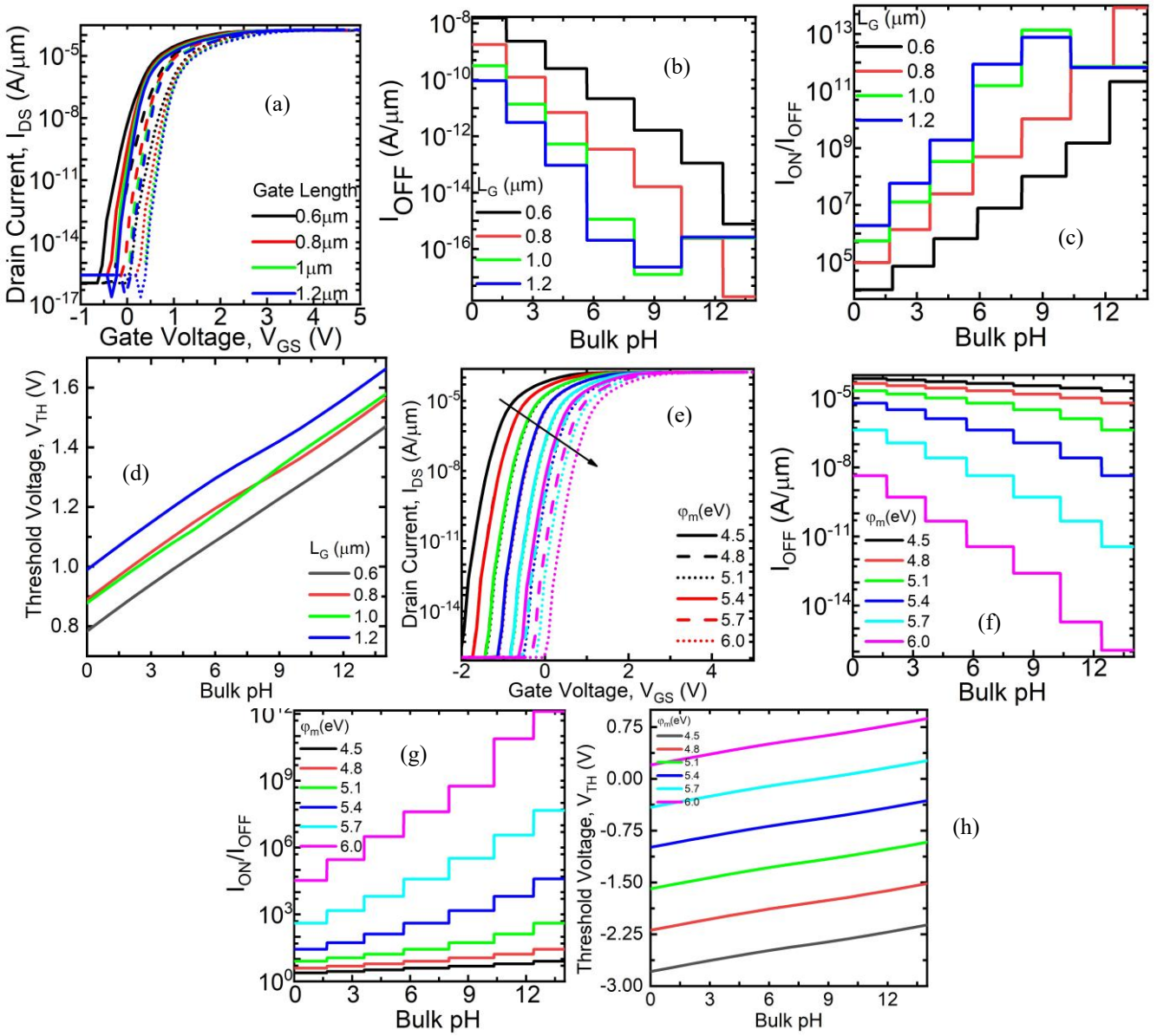



Fig. 4. (a) Transfer charcateritcs (b) $I_{OFF}$ (c) $I_{ON}/I_{OFF}$ (d) Threshold voltage with gate length variation for different pH from 0 to 14. (e) Transfer charcateritcs (f) $I_{OFF}$ (g) $I_{ON}/I_{OFF}$ (h) Threshold voltage with gate work function for different pH from 0 to 14.

(gm2) is a measure of how the output of a device changes as the input changes. It represents the rate at which the output changes with respect to the input ($^{dI_{DS}^2}/_{d\,V_{GS}^2}$). In linearity analysis, the second derivative is used to assess the degree of non-

linearity in the device, which can be caused by changes in input. If the second derivative is zero, it means the output changes linearly with the input and the device is considered linear. If the second derivative is non-zero, it means the output changes non-linearly with the input, indicating non-linear behavior of the device. For better linearity, gm2 should be lower since gm is shifted in the right direction with pH without any change in gm value. So, the peak value of gm2 is observed in the voltage between 2 V to 2.8V, as shown in Fig 3 (b).

In non-linearity analysis, the third derivative (gm3) can provide insight into the shape of the device's transfer function, which describes how the output changes as a function of the input ($^{dI_{DS}{}^3}/_{d\,V_{GS}{}^3}$). The third derivative can be used to quantify the curvature of the transfer function and provide information about how the device responds to changes in input. This information is important for applications that require precise control over the output of the device, such as communication systems or control systems. The value of gm3 is constant for all pH but the peak is obtained at a different voltage. Its value is larger and peak value is 0.0005 S/V2 plotted in Fig 3 (c).

Input intercepts point 3 (IIP3) is a measure of the linearity of a device and is used to determine the maximum input power level that can be applied to a device without causing significant distortion of the output signal. IIP3 is a performance parameter used to describe the linearity of an electronic device such as an amplifier, mixer, or ADC (c) such as in communication systems or in applications that require high signal quality. A higher IIP3 indicates better linearity and the ability to handle higher input power levels without significant distortion. It is defined as the input power level at which the output power level deviates from linearity by 3 dB. Fig 3 (d) plotted the graph of IIP3 with respect to $V_{GS}$ for pH 0 to 14. pH value does not affect the value of IIP3, it only shifts the same value from left to right.

Intermodulation distortion (IMD) is a type of non-linearity that results in the generation of additional frequency components in the output signal, which can interfere with the intended signal and result in distortion. It is an important factor in linearity analysis and is used to assess the quality of the output signal and the degree of linearity in a device. A low level of IMD indicates better linearity, while a high level of IMD indicates poor linearity and a need for improvement. Larger pH shows lower IMD and it is plotted in Fig. 3 (e).

## IV. Effects of design parameters on the performance

In this section, the β-AGO/GO HEMT device has been investigated at a constant temperature of 300K with a different pH value of electrolyte solution. Various analog parameters have been analyzed with different device parameters such as gate length (LG) and gate work function (ϕm).

### A. Effect of Gate length (LG) variation on pH:-

The β-AGO/GO HEMT-based pH sensor has been analyzed at different LG and the device's performance varies with pH. LG varies from 600nm to 1200nm with a step length of 200nm. Fig 4 (a) shows the different pH graphs between IDS and VGS. In all the simulated graphs, black, red, green and blue colors represent LG 600nm, 800nm, 1000nm and 1200nm, respectively. In transfer characteristics solid line represents lower pH (0), dash line shows pH (7), and the dotted line represents pH (14). Since the pH value does not affect the saturation value of the device. High gate voltage requires to the formation of channel with increase in gate length and so threshold voltage increases. Due to the larger H+ conc. at lower pH, the device is ON at lower bias voltage and for higher pH, the conc. of OH- is larger. Fig 4 (b) is plotted the graph between $I_{OFF}$ and $V_{GS}$. At lower LG, $I_{OFF}$ is large for all pH value and its value increases with LG. Since $I_{OFF}$ is varied with pH but the saturation value is constant, so $I_{ON}/I_{OFF}$ is also lower for small LG and increases with LG for all pH, and the graph of $I_{ON}/I_{OFF}$ is shown in Fig 4 (c). Threshold voltage increases with pH because the $I_{DS}$-$V_{GS}$ curve shifts in a rightward direction. So, lower $V_{TH}$ is observed for lower pH, and maximum for higher pH and the plot between $V_{TH}$ and bulk pH is shown in Fig. 4 (d). $V_{TH}$ also enhances with an increase in LG. Since $I_{DS}$ graph shifts to the right side of transfer characteristics.

### B. Effect of gate work function (ϕm) variation on pH: -

Device performance depends upon gate work function, ϕm, and it also alters the sensor behaviour. All the simulations of pH sensors with ϕm varied from 4.5 eV to 6.0 eV with a step size of 0.3 eV. Black, red, green, blue, cyan and pink colors represent ϕm variation 4.5 eV, 4.8 eV, 5.1 eV, 5.4 eV, 5.7eV and 6.0 eV, respectively. Fig. 4 (e) shows the transfer characteristics of the device with pH. The solid line shows pH value 0, dash line for pH 7 and a dotted line for pH 14. At lower ϕm, the device will deplete less in OFF-state condition, and switching speed is faster in the ON-state condition, and the device will be ON in the negative gate bias condition. If we increase the ϕm, the IDS versus VGS graph will shift in a positive direction therefore, device behavior changes from Normally-ON to Normally-OFF condition. At higher pH, the conc. of H+ is lower than the device will take a longer time for ON and time reduces for lower pH. pH does not affect the ON-state current. $I_{OFF}$ depends on pH value, and it decreases with pH. If we increase the ϕm, $I_{OFF}$ decreases and as shown in Fig 4(f). OFF-state current will depend on the pH, therefore, $I_{ON}/I_{OFF}$ is inversely related to $I_{OFF}$, and it describes in Fig 4 (g). Since $I_{DS}$-$V_{GS}$ shifted in the right direction with pH and ϕm. $V_{TH}$ increases with pH and ϕm. For lower pH, its value is lower and increases with pH value, as shown in Fig 4 (h). A comparision table II shows the with other ion-sensitive devices

Table II. Comparison with Ph sensor devices

| References | VTH/pH (mV) | IOFF (A/m) |
|---|---|---|
| [31] | 102 | 7.6×109 |
| [32] | 60 | 8 × 109 |
| [33] | 50 | - |
| [34] | 58.2 | - |
| [24] | 50.9 | 7.1 × 109 |
| This work | 50.2 | 7.9 × 109 |

## V. Conclusion

We analyzed a mathematical model under non-ideal conditions for a β-$(AlGa)_2O_3/Ga_2O_3$ HEMT-based ISFET pH sensor and examined its analog performance in relation to key device parameters, such as gate length and gate work function. An electrolyte layer was introduced between the gate metal and the $Al_2O_3$ oxide layer, where the electrical double layer forms at the interface. The linearity performance of the sensor was also explored in detail. All device simulations were conducted for pH values ranging from 0 to 14, covering both acidic and basic regions. $Al_2O_3$ served as both a passivation layer and a sensing membrane. The variation in the oxide surface potential altered the carrier concentration in the 2DEG, leading to changes in the drain current. We observed that the threshold voltage increased with pH, exhibiting a sensitivity of 54.3 mV/pH. Furthermore, as the gate work function varied with pH, the device transitioned from Normally-ON to Normally-OFF operation, significantly impacting its performance. These findings highlight the strong dependence of the pH sensor's behavior on gate length, work function, and pH, and provide important insights for optimizing its performance in a wide range of pH environments.

**Conflict of interest:** The authors declare that they have no conflict of interest.

**Authors' contributions**

**Ravi Ranjan:** Simulation, TCAD Software, Analytical modelling Writing- Original draft preparation.

**Ashish Raman:** TCAD Software, Writing- Original draft preparation.

**Nitesh Kashyap:** Simulation, Data curation and Revision.

**Naveen Kumar:** Simulation, TCAD Software, Logical-Methodology, conceptualization.

**Prateek Kumar :** Validation, Methodology

**Data Availability Statement:** Data will be provided on reasonable request.

## References


[1] Zhang A.P., Johnson J.W., Ren F.: 'Lateral AlxGa12xN power rectifiers with 9.7 kV reverse breakdown voltage', Appl. Phys. Lett., 78, pp. 823–825 (2001).

[2] Fei XX, Wang Y, Luo X, Cao F, Yu CH. Potential study of the enhanced breakdown voltage GaN MISFET based on partial AlN buried layer. Superlattices Microstruct;114:314–7 (2018).

[3] Bergveld, P. Development of an ion-sensitive solid-state device for neurophysiological measurements. IEEE Transactions on biomedical engineering, (1), pp.70-71 (1970)

[4] Medina-Bailon, C., Kumar, N., Dhar, R.P.S., Todorova, I., Lenoble, D., Georgiev, V.P. and García, C.P. Comprehensive analytical modelling of an absolute pH sensor. Sensors, 21(15), p.5190 (2021).

[5] Nair, P.R. and Alam, M.A., 2008. Screening-limited response of nanobiosensors. Nano letters, 8(5), pp.1281-1285.

[6] Kulkarni, G.S. and Zhong, Z. Detection beyond the Debye screening length in a high-frequency nanoelectronic biosensor. Nano letters, 12(2), pp.719-723 (2012).

[7] Zhang, J.; Rupakula, M.; Bellando, F.; Garcia Cordero, E.; Longo, J.; Wildhaber, F.; Herment, G.; Guérin, H.; Ionescu, A.M. Sweat Biomarker Sensor Incorporating Picowatt, Three-Dimensional Extended Metal Gate Ion Sensitive Field Effect Transistors. ACS Sens, 4, 2039–2047 (2019).

[8] Sakata, T. Biologically Coupled Gate Field-Effect Transistors Meet in Vitro Diagnostics. ACS Omega, 4, 11852–11862 (2019).

[9] Hashim, U.; Chong, S.W.; Liu, W.W. Fabrication of Silicon Nitride Ion Sensitive Field-Effect Transistor for pH Measurement and DNA Immobilization/Hybridization. J. Nanomater, 2013, 542737 (2013).

[10] Romele, P.; Gkoupidenis, P.; Koutsouras, D.A.; Lieberth, K.; Kovács-Vajna, Z.M.; Blom, P.W.M.; Torricelli, F. Multiscale real time and high sensitivity ion detection with complementary organic electrochemical transistors amplifier. Nat. Commun, 11, 3743 (2020).

[11] Pal, P., Pratap, Y., Gupta, M. and Kabra, S.Analytical modeling and simulation of AlGaN/GaN MOS-HEMT for high sensitive pH sensor. IEEE Sensors Journal, 21(12), pp.12998-13005 (2021).

[12] H. Yuan, H.-C. Kwon, S.-H. Yeom, D.-H. Kwon, and S.-W. Kang, "MOSFET–BJT hybrid mode of the gated lateral bipolar junction transistor for C-reactive protein detection," Biosensors Bioelectron., vol. 28, no. 1, pp. 434–437, Oct. (2011).

[13] N. Sharma et al., "High-resolution AlGaN/GaN HEMT-based electrochemical sensor for biomedical applications," IEEE Trans. Electron Devices, vol. 67, no. 1, pp. 289–295, Jan. (2020).

[14] N. Espinosa, S. U. Schwarz, V. Cimalla, and O. Ambacher, "Detection of different target-DNA concentrations with highly sensitive AlGaN/GaN high electron mobility transistors," Sens. Actuators B, Chem., vol. 210, pp. 633–639, Apr. (2015).

[15] J. Sun, R. Sokolovskij, E. Iervolino, Z. Liu, P. M. Sarro, and G. Zhang, "Suspended AlGaN/GaN HEMT NO2 gas sensor integrated with microheater," J. Microelectromech. Syst., vol. 28, no. 6, pp. 997–1004, Dec. (2019).

[16] C. Bishop et al., "Experimental study and device design of NO, NO2, and NH3 Gas detection for a wide dynamic and large temperature range using Pt/AlGaN/GaN HEMT," IEEE Sensors J., vol. 16, no. 18, pp. 6828–6838, Sep. (2016)

[17] S. Mostafa et al., "Integrated MOSFET-embedded-cantilever-based biosensor characteristic for detection of anthrax simulant," IEEE Electron Device Lett., vol. 32, no. 3, pp. 408–410, Mar. (2011)

[18] S. M. U. Ali, O. Nur, M. Willander, and B. Danielsson, "Glucose detection with a commercial MOSFET using a ZnO nanowires extended gate," IEEE Trans. Nanotechnol., vol. 8, no. 6, pp. 678–683, Nov. (2009).

[19] B.-H. Chu et al., "Chloride ion detection by InN gated AlGaN/GaN high electron mobility transistors," J. Vac. Sci. Technol. B, Microelectron., vol. 28, no. 1, pp. L5–L8, Jan. (2010)

[20] Ranjan, R., Kashyap, N. and Raman, A.. Demonstration of Temperature-Dependent Analysis of GAA–β-(AlGa) 2O3/Ga2O3 High Electron Mobility Transistor. IETE Journal of Research, pp.1-9 (2022).

[21] Ranjan, R., Kashyap, N. and Raman, A.,. Design and investigation of field plate-based vertical GAA–β-(AlGa) 2O3/Ga2O3 high electron mobility transistor. Micro and Nanostructures, 164, p.107117 (2022).

[22] Baur, B., Howgate, J., Von Ribbeck, H.G., Gawlina, Y., Bandalo, V., Steinhoff, G., Stutzmann, M. and Eickhoff, M.,. Catalytic activity of enzymes immobilized on Al Ga N⁄ Ga N solution gate field-effect transistors. Applied Physics Letters, 89(18), p.183901 (2006).

[23] Alifragis, Y., Volosirakis, A., Chaniotakis, N.A., Konstantinidis, G., Iliopoulos, E. and Georgakilas, A.. AlGaN/GaN high electron mobility transistor sensor sensitive to ammonium ions. physica status solidi (a), 204(6), pp.2059-2063 (2006).

[24] Ranjan, R., Kashyap, N. and Raman, A. Design and Analytical Assessment of Non-Ideal Ion-Sensitive β-MIS-(AlGa) 2 O 3/Ga 2 O 3 High Electron Mobility Transistor. IEEE Transactions on Nanotechnology (2023).

[25] Bandiziol, A., Palestri, P., Pittino, F., Esseni, D. and Selmi, L. A TCAD-based methodology to model the site-binding charge at ISFET/electrolyte interfaces. IEEE Transactions on Electron Devices, 62(10), pp.3379-3386 [2015].

[26] D. Welch, S. Shah, S. Ozev, and J. B. Christen, "Experimental and simulated cycling of ISFET electric fields for drift reset," IEEE Electron Device Lett., vol. 34, no. 3, pp. 456–458, Mar. (2013).

[27] S. Martinoia, G. Massobrio, and L. Lorenzelli, "Modeling ISFET microsensor and ISFET-based microsystems: A review," Sens. Actuators B, Chem., vol. 105, no. 1, pp. 14–27,(2005)

[28] Xue, D., Zhang, H., ul Ahmad, A., Liang, H., Liu, J., Xia, X., Guo, W., Huang, H. and Xu, N. Enhancing the sensitivity of the reference electrode free AlGaN/GaN HEMT based pH sensors by controlling the threshold voltage. Sensors and Actuators B: Chemical, 306, p.127609 (2020).

[29] Bandiziol, A., Palestri, P., Pittino, F., Esseni, D. and Selmi, L. A TCAD-based methodology to model the site-binding charge at ISFET/electrolyte interfaces. IEEE Transactions on Electron Devices, 62(10), pp.3379-3386 (2015).

[30] D. Welch, S. Shah, S. Ozev, and J. B. Christen, “Experimental and simulated cycling of ISFET electric fields for drift reset,” IEEE Electron Device Lett., vol. 34, no. 3, pp. 456–458, Mar. (2013).
[31] Narang, R., Saxena, M. and Gupta, M. Analytical model of pH sensing characteristics of junctionless silicon on insulator ISFET. IEEE Transactions on Electron Devices, 64(4), pp.1742-1750 (2017).
[32] Rusu, A., Hierlemann, A. and Ionescu, A.M, September. Low power finfet ph-sensor with high-sensitivity voltage readout. In 2013 Proceedings of the European Solid-State Device Research Conference (ESSDERC) (pp. 350-353). IEEE (2013).
[33] Chou, J.C. and Chiang, J.L. Ion sensitive field effect transistor with amorphous tungsten trioxide gate for pH sensing. Sensors and Actuators B: Chemical, 62(2), pp.81-87 (2000).
[34] Parmar, J.S., Bhat, A., Shafi, N., Porwal, A., Periasamy, C. and Sahu, C.,. Analysis of Current Drift in Al 2 O 3 Gated Junctionless pH Sensitive Field Effect Transistor. In 2021 IEEE International Symposium on Smart Electronic Systems (iSES)(Formerly iNiS) (pp. 131-134). IEEE (2021).